

UC Irvine

UC Irvine Previously Published Works

Title

A DFT Perspective on Organometallic Lanthanide Chemistry

Permalink

<https://escholarship.org/uc/item/6436r4mf>

Authors

Rajabi, Ahmadsreza

Grotjahn, Robin

Rappoport, Dmitriy

et al.

Publication Date

2023-11-01

DOI

10.1039/d3dt03221c

Copyright Information

This work is made available under the terms of a Creative Commons Attribution-NonCommercial-NoDerivatives License, available at <https://creativecommons.org/licenses/by-nc-nd/4.0/>

Peer reviewed

Cite this: DOI: 00.0000/xxxxxxxxxx

A DFT Perspective on Organometallic Lanthanide Chemistry

Ahmadreza Rajabi^a, Robin Grotjahn^a, Dmitriy Rappoport^a, and Filipp Furche^{*a}Received Date
Accepted Date

DOI: 00.0000/xxxxxxxxxx

Computational studies of the coordination chemistry and bonding of lanthanides have grown in recent decades as the need for understanding the distinct physical, optical, and magnetic properties of these compounds increased. Density functional theory (DFT) methods offer a favorable balance of computational cost and accuracy in lanthanide chemistry and have helped to advance the discovery of novel oxidation states and electronic configurations. This *Frontier* article examines the scope and limitations of DFT in interpreting structural and spectroscopic data of low-valent lanthanide complexes, elucidating periodic trends, and predicting their properties and reactivity, presented through selected examples.

1 Introduction

The coordination chemistry of lanthanides was long thought to offer limited variety and hold few surprises.^{1,2} Until recently, the majority of the coordination compounds of lanthanides were Ln³⁺ complexes with the 4f^{*n*} electronic configuration (*n* = 1 – 14 for Ce–Lu). Low-valent lanthanide compounds were known for several Ln²⁺ ions (Ln = Eu, Yb, Sm, and later Tm, Dy, and Nd) having the 4f^{*n*+1} configuration. The compact and core-like 4f shell was not expected to play a role in ligand bonding. However, over the past 15 years, the synthesis and characterization of new complexes containing divalent lanthanide ions^{3–7} and related reduced complexes^{8,9} have upended this conventional wisdom. The biggest surprise was that, in an appropriate ligand environment, 4f^{*n*}5d¹ orbital occupation may become feasible in the so-called unconventional Ln²⁺ ions. The 5d orbitals in these ions have greater spatial extent and overlap significantly with ligand orbitals, thus presenting new opportunities for coordination chemistry^{6,10–12} and enabling unique chemical reactivity^{13–16} and magnetic properties.^{17–20} We discuss examples of structures, molecular properties, and reactivities of low-valent lanthanide complexes in the following. The first completed series of divalent lanthanide complexes utilized the silyl-substituted cyclopentadienyl ligand Cp' = C₅H₄SiMe₃ and showed a new periodic trend of conventional (4f^{*n*+1}) and unconventional Ln²⁺ ions.^{21–23} Several further series of divalent lanthanide complexes have since been synthesized, including complexes of Cp'' = 1,3-C₅H₃(SiMe₃)₂,^{10,24} Cp^{tet} = C₅Me₄H,¹¹ silylamide N(SiMe₃)₂,¹² and aryloxy lig-

ands ((^{Ad,Me}ArO)₃Mes)^{3–},²⁵

Quantum chemical modeling has played an essential role in understanding low-valent lanthanide complexes. Computational studies suggested and helped confirm the 5d occupation in the unconventional Ln²⁺ ions; moreover, they were also used to elucidate the bonding, molecular properties, and reactions of the new complexes. Low-valent lanthanide complexes also present some distinct challenges for quantum chemical methods. As a result of the near-degeneracy of the 4f, 5d, and 6s shells in unconventional Ln²⁺ ions,^{21–23} the description of their electronic states is sensitive to the treatment of electron correlation. Similar to transition metal compounds,^{26–28} multiple spin states may be energetically accessible in lanthanide complexes. Moreover, relativistic effects are significant in lanthanide atoms and require the use of relativistic effective core potentials (ECPs) or relativistic all-electron approaches.^{29–34} In practice, the size of many lanthanide complexes severely limits the computationally feasible options, leaving Kohn–Sham density functional theory (KS-DFT) with density functional approximations (DFAs) as the most attractive compromise between performance and accuracy. Compared to the main-group elements and transition metals,^{35–40} the computational literature on lanthanide-containing molecules is still relatively sparse. Early computational studies of lanthanide compounds were reviewed in 1994 by Balasubramanian²⁹ and in 1996 by Dolg.⁴¹ The reviews by Dolg,⁴² Neese and co-workers,⁴³ and Kerridge⁴⁴ survey the current state of computational modeling of lanthanide compounds.

In this *Frontier* article, we focus on the interplay between computation and experiment in lanthanide chemistry using selected examples from this research group's work over the past decade. The selection of the examples reflects our personal, biased per-

^a Department of Chemistry, University of California Irvine, 1102 Natural Sciences II, Irvine, CA 92697-2025, USA. E-mail: filipp.furche@uci.edu

spective, and is not meant to be comprehensive; rather we aim to illustrate how DFT can be used as a tool for analyzing structural and spectroscopic data of low-valent lanthanide complexes, describing periodic trends, and computing their properties and reactions. While molecular complexes of tetravalent lanthanides Ce, Pr, and Tb are receiving increasing interest, we do not consider them in this review.^{45–47} The present perspective focuses on observables with a unique experimental definition; the reader is referred to more specialized papers for a discussion of “soft” concepts such as covalency^{48–53} and oxidation states.^{54,55} Our examples use the TURBOMOLE quantum chemistry suite⁵⁶ as the computational vehicle, however, many functionalities described here are available in any modern quantum chemistry program.

2 The Quantum Chemical Toolbox for Lanthanides

Multi-reference methods such as complete active space self-consistent field (CASSCF)⁵⁷ are frequently used to model lanthanides and their compounds.^{43,44} These approaches explicitly represent the effect of the static correlation due to the partial filling of the 4f shell in lanthanides and the competition with the 5d and 6s orbitals. However, a major drawback of CAS methods is that the choice of the active space is non-trivial^{58,59} and may introduce uncontrolled errors. For example, for an accurate description of the 4f correlation in late lanthanides, one has to include an additional f shell in the active space (double-shell effect).^{60,61} Moreover, dynamic correlation is insufficiently captured by CASSCF, while its treatment by second-order perturbation theory (CASPT2^{60,62} or NEVPT2⁶³) incurs additional computational cost. The steep increase of the computational cost with the size of the active space limits the scope of applications of CAS methods and requires compromises in other aspects of the computational methodology, for example, basis sets, structural relaxation, and characterization of molecular stability by Hessian calculations. Contrary to conventional wisdom, single-reference methods can accurately describe multiconfigurational states when used appropriately, e.g., in the spin-flip EOM framework.^{64,65}

Often, but not always, KS-DFT methods offer a favorable balance, which makes them a practical tool for calculations of larger lanthanide-containing molecules. In particular, the meta-generalized gradient approximation (mGGA) TPSS functional⁶⁶ and hybrid-mGGA TPSSh functional⁶⁷ have proven successful for transition metal chemistry^{68,69} as well as recent benchmarks of lanthanide molecules and complexes.^{70–72} In these studies, TPSS showed the lowest mean absolute error (MAE) of 19 kcal/mol for a set of enthalpies of formation and bond dissociation energies (B3LYP: 28 kcal/mol)⁷⁰ while TPSSh gave the lowest MAE for lanthanide-ligand bond lengths (0.069 Å vs. B3LYP: 0.162 Å).⁷²

Shortcomings of DFAs in modeling lanthanide compounds include the treatment of long-range nonbonding interactions such as van der Waals forces is a significant limitation of KS-DFT that can only be partially corrected empirically.^{73,74} Methods based on the random-phase approximation (RPA)⁷⁵ account for medium-range and long-range dispersion at moderate computational cost.^{75–78} The accurate description of spin-state splittings of metal complexes remains challenging, although hybrid func-

tionals with reduced amounts of exact-exchange (EXX) such as TPSSh tend to give better accuracy in comparison to standard hybrid functionals.^{26,79} This is closely linked to self-interaction errors in DFAs, which also show up in inaccurate s-d energy differences of atoms,⁸⁰ or ligand-field and certain CT transitions in time-dependent DFT (TDDFT) calculations.⁸¹ Local hybrid functionals with position-dependent EXX admixture may provide a more balanced description⁸² as has been demonstrated in studies of mixed-valence transition metal complexes.⁸³ RPA with exchange corrections⁷⁷ is also less prone to self-interaction error, albeit significantly more computationally demanding. Relativistic effects in lanthanide compounds may be treated by relativistic all-electron calculations^{29,30} or using relativistic ECPs.^{31,33} Both large-core ECPs, which include 4f orbitals in the core,³¹ and small-core ECPs allowing for flexible 4f occupations⁸⁴ are available for lanthanides. Several families of lanthanide basis sets have been developed for all-electron calculations^{85–87} and calculations with ECPs.^{88–90} Exact two-component (X2C) methods^{91–93} enable an efficient and accurate relativistic all-electron treatment for heavy elements including spin-orbit coupling. All-electron calculations typically require large uncontracted basis sets.^{85,86} Calculations of molecular properties depending on the structure of the core electron shells, such as electron-nucleus hyperfine coupling constants,⁹⁴ require relativistic treatment.

The KS-DFT calculations of lanthanide complexes, especially those with unconventional configurations, often suffer from slow convergence and metastable solutions. Therefore, one should not assume straightforward convergence to the stable electronic state and should always verify the orbital occupations of the converged solution. It is critically important to systematically explore different spin multiplicities and test the solutions for electronic stability. An unbiased starting point for KS-DFT calculations may be obtained by fractional occupation (Fermi smearing) calculations.^{95,96} To speed up convergence, increased SCF damping and level shifting⁹⁷ can be employed in combination with direct inversion in iterative space (DIIS) extrapolation;⁹⁸ however, these techniques also carry an increased risk of yielding metastable solutions.

3 Examples

3.1 Characterization of novel electronic configurations

The search for novel oxidation states of lanthanides generated great interest in reactions of molecular compounds of Ln²⁺ (Ln = Tm, Dy, Nd) with alkali metal salts of anionic ligands KC₅Me₅, NaN(SiMe₃)₂, KOAr (Ar = C₆H₃tBu₂).⁶ The resulting reaction mixtures are strongly reducing and capture molecular nitrogen as complexes of (N=N)²⁻. However, the reaction of DyI₂ with KOAr and nitrogen gave not only the (N₂)²⁻-containing product but also complexes [(ArO)₂(THF)Dy]₂(μ-η²:η²-N₂)[K(THF)₆] and [(ArO)₂(THF)Dy]₂(μ³-η²:η²:η²-N₂)K(THF), which suggested the presence of the previously unobserved (N₂)³⁻ radical anion as part of the Dy₂N₂ group.⁸ Analogous complexes were also obtained with Y and Ln = Lu, Er, La ions and N(SiMe₃)₂ ligands.^{8,9,99}

The combination of experimental electronic paramagnetic res-

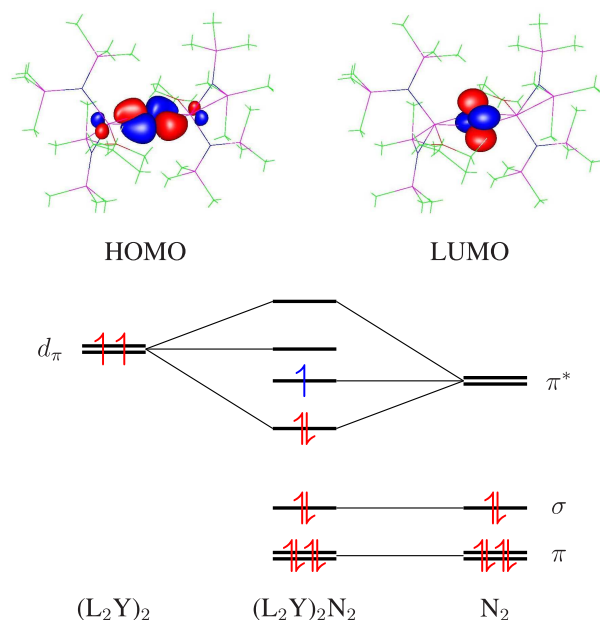


Fig. 1 Simplified MO diagram of $[\text{L}_2\text{Y}_2(\mu\text{-}\eta^2\text{:}\eta^2\text{-N}_2)]^y$ complexes ($\text{L} = \text{N}(\text{SiMe}_3)_2$, $y = 0, -1$). Orbital occupations in the $y = 0$ complex are shown in red. The formation of the $\text{Y}(\text{d}_\pi)\text{-N}(\pi^*)$ bond is indicated by solid lines. The unpaired electron in the $y = -1$ complex is shown in blue. Reprinted with permission from Ref. 8. Copyright 2009 American Chemical Society.

onance (EPR) and Raman studies and DFT calculations of the $[\{(\text{Me}_3\text{Si})_2\text{N}\}_2(\text{THF})\text{Y}\}_2(\mu\text{-}\eta^2\text{:}\eta^2\text{-N}_2)]^y$ complexes ($y = 0, -1$) helped to establish their electronic configurations and the structure of the N_2 bridge.⁸ Calculations using the TPSSh functional⁶⁷ confirmed the localization of the unpaired electron in the N_2 π^* orbital of the $y = -1$ complex, as shown in Fig. 1.⁸ The analysis of the frontier molecular orbitals (MOs) of the $y = 0, -1$ complexes indicated a polar covalent interaction between Y^{2+} ions and the N_2 group consistent with a two-electron four-center bond. This bond is formed by back donation of d^1 orbitals of Y^{2+} into empty π^* orbitals of N_2 . The $[(\text{Me}_3\text{Si})_2\text{N}]_2\text{Y}$ fragments have a near-zero formal charge, which further underscored the covalent character of these interactions. The bonding orbital of the two-electron four-center bond in the highest occupied MO (HOMO) of the $y = 0$ complex. The corresponding lowest unoccupied MO (LUMO) is essentially an unperturbed π^* orbital of N_2 , oriented perpendicular to the Y_2N_2 plane. In the $y = -1$ complex, the π^* orbital is singly occupied, which reduces the formal N–N bond order from 2 to 1.5. As a result, the N–N vibrational frequency is predicted to decrease from 1425 cm^{-1} to 989 cm^{-1} , in agreement with the experimental Raman data.⁸ Additional evidence for the presence of a divalent metal intermediate in the synthesis pathway of $(\text{N}_2)^{2-}$ and $(\text{N}_2)^{3-}$ complexes of Y was obtained from EPR measurements of a blue solution of $\text{Y}[\text{N}(\text{SiMe}_3)_2]_3/\text{KC}_8$ in THF under argon at $-78\text{ }^\circ\text{C}$. The EPR spectra displayed a doublet pattern consistent with EPR parameters of Y^{2+} species.¹⁰⁰

Table 1 Experimental X-ray and DFT average M–Cp' centroid distances in $[\text{MCp}'_3]^y$ complexes (\AA , $\text{Cp}' = \text{C}_5\text{H}_4\text{SiMe}_3$, $y = 0, -1$). The distances are given as $[\text{MCp}'_3] (\text{M}^{3+}) / [\text{MCp}'_3]^- (\text{M}^{2+})$. * indicates unconventional, † indicates conventional M^{2+} complexes. Adapted from Ref. 22. Copyright 2013 American Chemical Society.

M	Experiment		DFT	
	(M–Cp') _{avg}	difference	(M–Cp') _{avg}	difference
Y*	2.405/2.436	0.031	2.416/2.446	0.030
Pr*	2.508/2.535	0.027	2.556/2.590	0.034
Gd*	2.437/2.468	0.031	2.479/2.502	0.023
Tb*	2.423/2.454	0.031	2.460/2.493	0.033
Ho*	2.394/2.426	0.032	2.437/2.466	0.029
Er*	2.386/2.416	0.030	2.422/2.454	0.032
Lu*	2.361/2.392	0.031	2.361/2.385	0.024
Sm†	2.461/2.608	0.147	2.470/2.600	0.130
Eu†	2.451/2.607	0.156	2.485/2.604	0.117
Tm†	2.379/2.502	0.123	2.385/2.501	0.116

3.2 Analysis of trends across the lanthanide series

The experimental data from several series of M^{2+} complexes ($\text{M} = \text{Y}, \text{La}–\text{Lu}$ except Pm) with $\text{Cp}'^{21-23,100}$, $\text{N}(\text{SiMe}_3)_2$ ¹² and other ligands showed characteristic structural differences between conventional complexes containing M^{2+} ions with the $4f^{n+1}$ electronic configuration and unconventional complexes, in which the M^{2+} ions had the novel $4f^n5d^1$ configuration ($4d^1$ for Y).^{6,7} The differences between the structural and spectroscopic properties of these two classes were analyzed with the help of DFT and TDDFT calculations. Table 1 compares the experimental X-ray and DFT results for the average M–Cp' centroid distances in $[\text{MCp}'_3]^y$ complexes ($y = 0, -1$).^{21-23,100} The DFT calculations used the TPSSh functional⁶⁷ and def2-TZVP basis sets for the metals (def2-SV(P) for non-metals)^{88,101} together with small-core ECPs.⁸⁴ The elongation of the M–Cp' distance upon reduction from trivalent to divalent ions is $0.1\text{--}0.2\text{ \AA}$ in conventional complexes, but much smaller, between $0.02\text{--}0.05\text{ \AA}$, in unconventional complexes. The DFT results reproduced the experimental structures from X-ray crystallography to within 1–2%. As the analysis of the metal orbitals showed, the trigonal ligand environment of the $[\text{MCp}'_3]^-$ complexes stabilizes the d_{z^2} orbital and significantly reduces the $4f \rightarrow 5d$ promotion energy compared to the atomic M^{2+} ions.^{102,103}

A characteristic feature of the $5d^1$ orbital occupation in unconventional M^{2+} complexes is the strong absorption band in the visible range dominated by Laporte-allowed excitations from the $5d$ orbital. By contrast, optical absorption spectra of conventional M^{2+} complexes are due to $4f \rightarrow 4f$ excitations and are several orders of magnitude less intense. Fig. 2 shows experimental and simulated absorption spectra of conventional ($\text{M} = \text{Sm}, \text{Tm}$) and unconventional ($\text{M} = \text{Nd}, \text{La}$) complexes.²³ TDDFT calculations were performed using the TPSSh functional,⁶⁷ the COSMO implicit solvation model,¹⁰⁴ and def2-TZVP basis sets for the metals⁸⁸ (def2-SVPD for non-metals¹⁰⁵). The difference in the spectral intensities in the visible range is a reliable indicator of the electronic configuration.

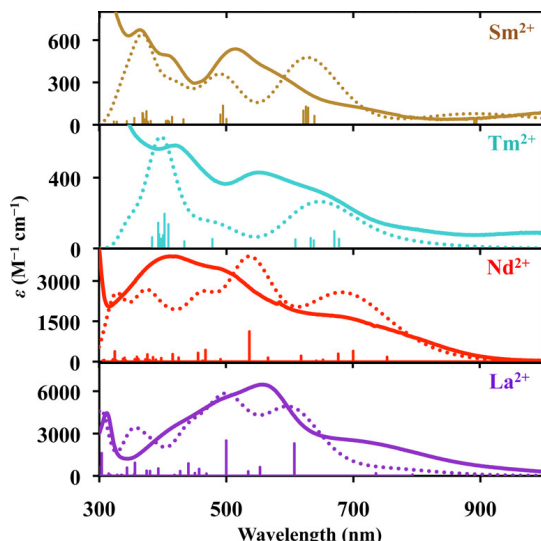


Fig. 2 Experimental UV/visible spectra of $[\text{MCp}_3]^-$ ($M = \text{Sm}, \text{Tm}, \text{Nd}, \text{La}$) in THF at 298 K (solid lines) and simulated spectra using TDDFT (spikes and dotted lines). Adapted with permission from Ref. 23. Copyright 2015 American Chemical Society.

3.3 Computational studies of molecular properties

DFT calculations enable predictions of the optical and magnetic properties of organolanthanide complexes of interest as single-molecule magnets (SMMs)^{106,107} or molecular spin qubits.^{108,109} For example, the use of the bulky pentaisopropylcyclopentadienyl (Cp^{iPr_3}) ligands results in lanthanide complexes with an axial ligand field, which enhances the anisotropy of the 4f shell.¹⁰⁶ The complexes $\text{M}(\text{Cp}^{\text{iPr}_3})_2$, where $M = \text{Tb}, \text{Dy}$, were the first examples of linear divalent lanthanide metallocenes exhibiting SMM properties.¹⁸ To probe the electronic structures of these complexes, DFT computations were used, exploring various potential spin states. Structure optimizations using the TPSS functional⁶⁶ including D3 dispersion correction⁷³ showed that the Tb complex has the ground term ^8A (in C_1 symmetry), while the ground term of the Dy complex is $^7\text{A}_1$ (in D_5 symmetry). The optimized structures were in good agreement with X-ray data. Both complexes exhibit unconventional $4f^8 5d^1$ configurations with pronounced s/d mixing, as illustrated in Fig. 3. Covalent σ bonding interactions between the metal-centric s/d orbital and ligand orbitals likely support the linear coordination geometry. The nondegenerate HOMO and the doubly degenerate LUMO are shown in Fig. 3.

DC magnetic susceptibility measurements have revealed that the $\chi_{\text{M}}T$ values for the divalent Tb^{2+} and Dy^{2+} in metallocenes differ from those observed in trigonal complexes. The experimental $\chi_{\text{M}}T$ value of the $\text{Tb}(\text{Cp}^{\text{iPr}_3})_2$ complex at room temperature is 12.72 emu·K/mol,¹⁸ which is notably lower than the values in trigonally coordinated unconventional Tb^{2+} complexes with $4f^8 5d^1$ configuration, for example, 13.73 emu·K/mol in $[\text{TbCp}_3]^-$ ¹⁷ and 14.83 emu·K/mol in $\{\text{Tb}[\text{N}(\text{SiMe}_3)_2]_3\}^-$.¹²

3.4 Predictions of lanthanide reactivity

Photochemical activation of trivalent lanthanide complexes is uncommon because their low-lying excited states correspond to

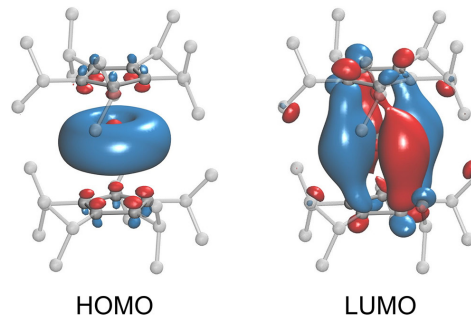


Fig. 3 Contour plots of the HOMO (left, $170\text{A}\alpha$) and LUMO (right, $172\text{A}\alpha$) of $\text{Tb}(\text{Cp}^{\text{iPr}_3})_2$. Contour value is 0.03. Hydrogen atoms are omitted for clarity. Adapted with permission from Ref. 18. Copyright 2019 American Chemical Society.

$4f \rightarrow 4f$ transitions, which are both Laporte-forbidden and have small vibronic couplings because of the compactness of the 4f shell. Due to the lack of couplings, these excited states usually decay by luminescence.^{110,111} However, recent studies reported photochemically induced reduction of N_2 by the mixed-ligand complexes $[(\text{C}_5\text{Me}_5)_{3-x}(\text{C}_5\text{Me}_4\text{H})_x\text{M}]$ ($M = \text{Y}, \text{Dy}, \text{Lu}; x = 1, 2$).^{13,112} The photochemical activity is due to the $(\eta^3\text{-C}_5\text{Me}_4\text{H})^-$ ligand with the unusual trihapto coordination. Electronic excitation in this ligand results in the intramolecular single electron transfer to the M^{3+} central ion, which generates an excited “ $(\text{C}_5\text{Me}_5)_2\text{M}^*$ ” complex with d^1 occupation and a $\text{C}_5\text{Me}_4\text{H}$ radical. The highly reducing M^{2+} complex acts as a reductant of N_2 .

The structures of the ground and excited states of the $[(\text{C}_5\text{Me}_5)_2(\text{C}_5\text{Me}_4\text{H})\text{M}]$ complexes ($M = \text{Y}, \text{Dy}$) were investigated by DFT and TDDFT calculations using the TPSSh functional⁶⁷, see Fig. 4a.¹³ The HOMO in these complexes was found to be localized on the $(\eta^3\text{-C}_5\text{Me}_4\text{H})^-$ ligand, in contrast to the corresponding homoleptic complexes, in which the HOMO was delocalized over all ligands. The comparison of the experimental and TDDFT UV/visible spectra of the photoactive $M = \text{Y}$ complexes are shown in Fig. 4b. The lower-energy band, identified in both experiment and simulation, is photochemically active in the mixed-ligand complex and is absent in its homoleptic analog. The ligand-to-metal charge transfer (LMCT) excitations in this band, occurring at 412 and 437 nm, correspond to transitions from the ligand-based HOMO to the LUMO with Y $4d_{z^2}$ character, as indicated by the structural changes in the excited state (Fig. 4a). The $4d^1$ excited state of the $(\text{C}_5\text{Me}_5)_2\text{Y}$ group is strongly reducing and can fix molecular nitrogen as N_2^{2-} . Mixed-ligand complexes containing $(\eta^3\text{-allyl})$ ligands, $[(\text{C}_5\text{Me}_5)_2(\eta^3\text{-C}_3\text{H}_5)\text{M}]$, where $M = \text{Y}, \text{Lu}$, were shown to reduce sulfur and polymerize isoprene upon photoactivation.¹⁴

4 Conclusions and Outlook

Density functional methods have been instrumental to the search for novel oxidation states and bonding patterns in lanthanide compounds. They enabled wide-ranging computational explorations that complemented experimental works and suggested new directions. For instance, the insight into the localization of the unpaired electron in the $(\text{N}_2)^{3-}$ bridging

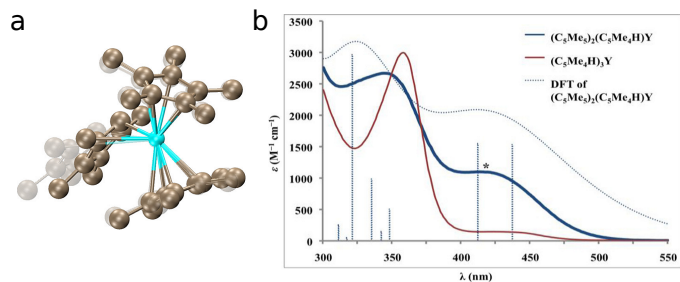


Fig. 4 a) Optimized geometries of the ground state (darkened) and first excited state (faded) of $(C_5Me_5)_2(C_5Me_4H)Y$. b) Experimental UV/visible spectra of $(C_5Me_5)_2(C_5Me_4H)Y$ (solid black line) and $(C_5Me_4H)_3Y$ (solid red line) and TDDFT spectrum of $(C_5Me_5)_2(C_5Me_4H)Y$ (dotted line and sticks). Reprinted with permission from Ref. 13. Copyright 2013 American Chemical Society.

group, which was obtained from the DFT analysis of the $[\{(Me_3Si)_2N\}_2(THF)Y\}_2(\mu-\eta^2:\eta^2-N_2)]^-$ complex,⁹ has led to the synthesis of bimetallic complexes $[\{(Me_3Si)_2N\}_2(THF)Ln_2(\mu-\eta^2:\eta^2-N_2)]^-$ ($Ln = Gd, Tb, Dy, Ho, Er$), with strong magnetic coupling between the metal centers mediated by the radical bridge.^{113,114} These complexes were found to have very large spin magnetic moments and to behave as single-molecule magnets (SMMs). Additionally, the novel electronic configurations in low-valent lanthanide complexes have been deployed for novel chemical reactivity, formation of metal–metal bonds,^{19,115} and the reduction of CO, CO₂, and N₂.^{116,117}

With the rapid advances in quantum technological applications,^{20,118} there is a growing need for efficient, predictive, and reliable quantum chemical methods to study the electronic structure of f-block element complexes. Given the large size, complexity of the electronic structure, relativistic effects, and spin-orbit coupling in organolanthanide complexes, coupled with the need to model solvent effects, DFT will continue to play a key role in the modeling of these compounds. The continued improvement and extension of computational methods for molecular property calculations, such as EPR⁹⁴ and NMR¹¹⁹, magnetic circular dichroism¹²⁰, and X-ray spectra^{121–123} is critical for further discovery and characterization of lanthanide-based materials.

Despite this positive outlook, DFT results should always be regarded with healthy skepticism. For example, agreement between a DFT-optimized structure and an experimental X-ray structure alone, however “perfect”, has little significance; at least one, but better two spectroscopic or magnetic properties should also be compared to experiment before reaching any conclusions. It is moreover vital to carefully cross-validate results between different theoretical methods, and avoid confirmation bias by viewing them in the context of previous calculations and known limitations.

Author Contributions

Ahmadreza Rajabi: Conceptualization (lead); Writing - Original Draft (lead); Visualization (lead); Writing - Review & Editing (lead). **Robin Grotjahn:** Writing - Original Draft (supporting); Writing/Review & Editing (supporting). **Dmitrij Rappoport:**

Conceptualization (supporting); Supervision (equal); Writing - Original Draft (equal); Writing - Review & Editing (equal). **Filipp Furche:** Conceptualization (lead); Supervision (lead); Writing - Original Draft (supporting); Writing - Review & Editing (supporting)

Conflicts of interest

The authors declare the following competing financial interest: Principal Investigator Filipp Furche has an equity interest in TUR-BOMOLE GmbH. The terms of this arrangement have been reviewed and approved by the University of California, Irvine, in accordance with its conflict of interest policies.

Acknowledgements

This material is based upon work supported by the National Science Foundation under CHE-2102568. R. G. acknowledges support via a Walter-Benjamin postdoctoral fellowship funded by the Deutsche Forschungsgemeinschaft (DFG, German Research Foundation) – 501114520. F.F. acknowledges helpful discussions and years of fruitful collaboration with William J. Evans. The Eddleman Quantum Institute is acknowledged for learning and collaboration opportunities.

Notes and references

- 1 L. Maron and O. Eisenstein, *J. Phys. Chem. A*, 2000, **104**, 7140–7143.
- 2 S. Cotton, *Lanthanide and Actinide Chemistry*, Wiley, Chichester, 2006.
- 3 M. N. Bochkarev, *Coord. Chem. Rev.*, 2004, **248**, 835–851.
- 4 F. Nief, *Dalton Trans.*, 2010, **39**, 6589–6598.
- 5 W. J. Evans, *J. Alloys Compd.*, 2009, **488**, 493–510.
- 6 D. H. Woen and W. J. Evans, *Handbook on the Physics and Chemistry of Rare Earths*, Elsevier, Amsterdam, 2016, vol. 50, ch. 293, pp. 337–394.
- 7 W. J. Evans, *Organometallics*, 2016, **35**, 3088–3100.
- 8 W. J. Evans, M. Fang, G. Zucchi, F. Furche, J. W. Ziller, R. M. Hoekstra and J. I. Zink, *J. Am. Chem. Soc.*, 2009, **131**, 11195–11202.
- 9 M. Fang, J. E. Bates, S. E. Lorenz, D. S. Lee, D. B. Rego, J. W. Ziller, F. Furche and W. J. Evans, *Inorg. Chem.*, 2011, **50**, 1459–1469.
- 10 C. T. Palumbo, L. E. Darago, C. J. Windorff, J. W. Ziller and W. J. Evans, *Organometallics*, 2018, **37**, 900–905.
- 11 T. F. Jenkins, D. H. Woen, L. N. Mohanam, J. W. Ziller, F. Furche and W. J. Evans, *Organometallics*, 2018, **37**, 3863–3873.
- 12 A. J. Ryan, L. E. Darago, S. G. Balasubramani, G. P. Chen, J. W. Ziller, F. Furche, J. R. Long and W. J. Evans, *Chem. Eur. J.*, 2018, **24**, 7702–7709.
- 13 M. E. Fieser, J. E. Bates, J. W. Ziller, F. Furche and W. J. Evans, *J. Am. Chem. Soc.*, 2013, **135**, 3804–3807.
- 14 M. E. Fieser, C. W. Johnson, J. E. Bates, J. W. Ziller, F. Furche and W. J. Evans, *Organometallics*, 2015, **34**, 4387–4393.
- 15 A. J. Ryan, S. G. Balasubramani, J. W. Ziller, F. Furche and W. J. Evans, *J. Am. Chem. Soc.*, 2020, **142**, 9302–9313.

- 16 A. B. Chung, A. J. Ryan, M. Fang, J. W. Ziller and W. J. Evans, *Inorg. Chem.*, 2021, **60**, 15635–15645.
- 17 K. R. Meihaus, M. E. Fieser, J. F. Corbey, W. J. Evans and J. R. Long, *J. Am. Chem. Soc.*, 2015, **137**, 9855–9860.
- 18 C. A. Gould, K. R. McClain, J. M. Yu, T. J. Groshens, F. Furche, B. G. Harvey and J. R. Long, *J. Am. Chem. Soc.*, 2019, **141**, 12967–12973.
- 19 C. A. Gould, K. R. McClain, D. Reta, J. G. C. Kragoskow, D. A. Marchiori, E. Lachman, E.-S. Choi, J. G. Analytis, R. D. Britt, N. F. Chilton, B. G. Harvey and J. R. Long, *Science*, 2022, **375**, 198–202.
- 20 K. Kundu, J. R. K. White, S. A. Moehring, J. M. Yu, J. W. Ziller, F. Furche, W. J. Evans and S. Hill, *Nat. Chem.*, 2022, **14**, 392–397.
- 21 M. R. MacDonald, J. E. Bates, M. E. Fieser, J. W. Ziller, F. Furche and W. J. Evans, *J. Am. Chem. Soc.*, 2012, **134**, 8420–8423.
- 22 M. R. MacDonald, J. E. Bates, J. W. Ziller, F. Furche and W. J. Evans, *J. Am. Chem. Soc.*, 2013, **135**, 9857–9868.
- 23 M. E. Fieser, M. R. MacDonald, B. T. Krull, J. E. Bates, J. W. Ziller, F. Furche and W. J. Evans, *J. Am. Chem. Soc.*, 2015, **137**, 369–382.
- 24 P. B. Hitchcock, M. F. Lappert, L. Maron and A. V. Protchenko, *Angew. Chem. Int. Ed.*, 2008, **120**, 1510–1513.
- 25 M. E. Fieser, C. T. Palumbo, H. S. La Pierre, D. P. Halter, V. K. Vooora, J. W. Ziller, F. Furche, K. Meyer and W. J. Evans, *Chem. Sci.*, 2017, **8**, 7424–7433.
- 26 O. Salomon, M. Reiher and B. A. Hess, *J. Chem. Phys.*, 2002, **117**, 4729–4737.
- 27 T. F. Hughes and R. A. Friesner, *J. Chem. Theory Comput.*, 2011, **7**, 19–32.
- 28 E. I. Ioannidis and H. J. Kulik, *J. Chem. Phys.*, 2015, **143**, 034104.
- 29 K. Balasubramanian, *Handbook on the Physics and Chemistry of Rare Earths*, Elsevier, Amsterdam, 1994, vol. 18, ch. 119, pp. 29–158.
- 30 J. Autschbach, S. Siekierski, M. Seth, P. Schwerdtfeger and W. H. E. Schwarz, *J. Comput. Chem.*, 2002, **23**, 804–813.
- 31 X. Cao and A. Weigand, in *Relativistic Pseudopotentials and Their Applications*, ed. M. Dolg, Wiley, Chichester, 2015, ch. 6, pp. 147–179.
- 32 T. Saue and L. Visscher, *Computational Methods in Lanthanide and Actinide Chemistry*, Wiley, Chichester, 2015, ch. 3, pp. 55–87.
- 33 M. Dolg and X. Cao, *Chem. Rev.*, 2012, **112**, 403–480.
- 34 J. Autschbach, *J. Chem. Phys.*, 2012, **136**, 150902.
- 35 T. Ziegler and J. Autschbach, *Chem. Rev.*, 2005, **105**, 2695–2722.
- 36 C. J. Cramer and D. G. Truhlar, *Phys. Chem. Chem. Phys.*, 2009, **11**, 10757–10816.
- 37 S. M. Tekarli, M. L. Drummond, T. G. Williams, T. R. Cundari and A. K. Wilson, *J. Chem. Phys. A*, 2009, **113**, 8607–8614.
- 38 W. M. C. Sameera and F. Maseras, *WIREs Comput. Mol. Sci.*, 2012, **2**, 375–385.
- 39 M. R. A. Blomberg, T. Borowski, F. Himo, R.-Z. Liao and P. E. M. Siegbahn, *Chem. Rev.*, 2014, **114**, 3601–3658.
- 40 K. D. Vogiatzis, M. V. Polynski, J. K. Kirkland, J. Townsend, A. Hashemi, C. Liu and E. A. Pidko, *Chem. Rev.*, 2019, **119**, 2453–2523.
- 41 M. Dolg and H. Stoll, *Handbook on the Physics and Chemistry of Rare Earths*, Elsevier, Amsterdam, 1996, vol. 22, ch. 152, pp. 607–729.
- 42 *Computational Methods in Lanthanide and Actinide Chemistry*, ed. M. Dolg, Wiley, Chichester, 2015.
- 43 D. Aravena, M. Atanasov and F. Neese, *Inorg. Chem.*, 2016, **55**, 4457–4469.
- 44 A. Kerridge, *The Lanthanides and Actinides*, World Scientific, 2022, pp. 549–574.
- 45 T. P. Gomba, A. Ramanathan, N. T. Rice and H. S. La Pierre, *Dalton Trans.*, 2020, **49**, 15945–15987.
- 46 M. A. Hay and C. Boskovic, *Chem. Eur. J.*, 2021, **27**, 3608–3637.
- 47 A. R. Willauer, I. Douair, A.-S. Chauvin, F. Fadaei-Tirani, J.-C. G. Bünzli, L. Maron and M. Mazzanti, *Chem. Sci.*, 2022, **13**, 681–691.
- 48 R. G. Denning, J. Harmer, J. C. Green and M. Irwin, *J. Am. Chem. Soc.*, 2011, **133**, 20644–20660.
- 49 M. L. Neidig, D. L. Clark and R. L. Martin, *Coord. Chem. Rev.*, 2013, **257**, 394–406.
- 50 M. W. Löble, J. M. Keith, A. B. Altman, S. C. E. Stieber, E. R. Batista, K. S. Boland, S. D. Conradson, D. L. Clark, J. Lezama Pacheco, S. A. Kozimor *et al.*, *J. Am. Chem. Soc.*, 2015, **137**, 2506–2523.
- 51 A. Kerridge, *Chem. Commun.*, 2017, **53**, 6685–6695.
- 52 J. Jung, M. Atanasov and F. Neese, *Inorg. Chem.*, 2017, **56**, 8802–8816.
- 53 T. Vitova, P. Roesky and S. Dehnen, *Commun. Chem.*, 2022, **5**, 12.
- 54 G. Meyer, *Angew. Chem. Int. Ed.*, 2014, **53**, 3550–3551.
- 55 M. Tricoire, N. Mahieu, T. Simler and G. Nocton, *Chem. Eur. J.*, 2021, **27**, 6860–6879.
- 56 Y. Franzke, C. Holzer, J. H. Andersen, T. Begušić, F. Bruder, S. Coriani, F. Della Sala, E. Fabiano, D. A. Fedotov, S. Fürst, S. Gillhuber, R. Grotjahn, M. Kaupp, M. Kehry, M. Kristić, F. Mack, S. Majumdar, B. D. Nguyen, S. M. Parker, F. Pauly, A. Pausch, E. Perlt, G. S. Phun, A. Rajabi, D. Rappoport, B. Samal, T. Schrader, M. Sharma, E. Tapavicza, R. S. Treß, V. Vooora, A. Wodyński, J. M. Yu, B. Zerulla, F. Furche, C. Hättig, M. Sierka, D. P. Tew and F. Weigend, *J. Chem. Theory Comput.*, 2023, **19**, 6859–6890.
- 57 B. O. Roos, *Ab Initio Methods in Quantum Chemistry, Part 2*, Wiley, New York, 1987, vol. 69, pp. 399–445.
- 58 S. Keller, K. Boguslawski, T. Janowski, M. Reiher and P. Pulay, *J. Chem. Phys.*, 2015, **142**, 244104.
- 59 J. J. Bao, S. S. Dong, L. Gagliardi and D. G. Truhlar, *J. Chem. Theory Comput.*, 2018, **14**, 2017–2025.
- 60 K. Pierloot, *Mol. Phys.*, 2003, **101**, 2083–2094.
- 61 Z. Barandiarán and L. Seijo, *J. Chem. Phys.*, 2013, **138**,

- 074102.
- 62 K. Andersson, P.-Å. Malmqvist and B. O. Roos, *J. Chem. Phys.*, 1992, **96**, 1218–1226.
- 63 C. Angeli, R. Cimiraglia and J.-P. Malrieu, *Chem. Phys. Lett.*, 2001, **350**, 297–305.
- 64 M. Alessio and A. I. Krylov, *J. Chem. Theory Comput.*, 2021, **17**, 4225–4241.
- 65 S. Kotaru, P. Pokhilko and A. I. Krylov, *J. Chem. Phys.*, 2022, **157**, 224110.
- 66 J. Tao, J. P. Perdew, V. N. Staroverov and G. E. Scuseria, *Phys. Rev. Lett.*, 2003, **91**, 146401.
- 67 V. N. Staroverov, G. E. Scuseria, J. Tao and J. P. Perdew, *J. Chem. Phys.*, 2003, **119**, 12129–12137.
- 68 F. Furche and J. P. Perdew, *J. Chem. Phys.*, 2006, **124**, 044103.
- 69 M. Bühl and H. Kabrede, *J. Chem. Theory Comput.*, 2006, **2**, 1282–1290.
- 70 S. Grimme, G. Schoendorff and A. K. Wilson, *J. Chem. Theory Comput.*, 2016, **12**, 1259–1266.
- 71 L. E. Aebersold, S. H. Yuwono, G. Schoendorff and A. K. Wilson, *J. Chem. Theory Comput.*, 2017, **13**, 2831–2839.
- 72 G. A. McCarver, R. J. Hinde and K. D. Vogiatzis, *Inorg. Chem.*, 2020, **59**, 10492–10500.
- 73 S. Grimme, J. Antony, S. Ehrlich and H. Krieg, *J. Chem. Phys.*, 2010, **132**, 154104.
- 74 E. Caldeweyher, S. Ehlert, A. Hansen, H. Neugebauer, S. Spicher, C. Bannwarth and S. Grimme, *J. Chem. Phys.*, 2019, **150**, 154122.
- 75 G. P. Chen, V. K. Voora, M. M. Agee, S. G. Balasubramani and F. Furche, *Annu. Rev. Phys. Chem.*, 2017, **68**, 421–445.
- 76 H. Eshuis, J. Yarkony and F. Furche, *J. Chem. Phys.*, 2010, **132**, 234114.
- 77 J. E. Bates and F. Furche, *J. Chem. Phys.*, 2013, **139**, 171103.
- 78 M. E. Fieser, T. J. Mueller, J. E. Bates, J. W. Ziller, F. Furche and W. J. Evans, *Organometallics*, 2014, **33**, 3382–3890.
- 79 M. Reimann and M. Kaupp, *J. Chem. Theory Comput.*, 2022, **18**, 7442–7456.
- 80 J. P. Perdew and A. Zunger, *Phys. Rev. B*, 1981, **23**, 5048–5079.
- 81 M. Rudolph, T. Ziegler and J. Autschbach, *Chem. Phys. Lett.*, 2011, **391**, 92–100.
- 82 T. M. Maier, A. V. Arbuznikov and M. Kaupp, *Wiley Interdiscip. Rev. Comput. Mol. Sci.*, 2019, **9**, e1378.
- 83 D. P. Harrison, R. Grotjahn, M. Naher, S. M. B. H. Ghazvini, D. M. Mazzucato, M. Korb, S. A. Moggach, C. Lambert, M. Kaupp and P. J. Low, *Angew. Chem. Int. Ed.*, 2022, **61**, e202211000.
- 84 M. Dolg, H. Stoll and H. Preuss, *J. Chem. Phys.*, 1989, **90**, 1730–1734.
- 85 P. Pollak and F. Weigend, *J. Chem. Theory Comput.*, 2017, **13**, 3696–3705.
- 86 Y. J. Franzke, L. Spiske, P. Pollak and F. Weigend, *J. Chem. Theory Comput.*, 2020, **16**, 5658–5674.
- 87 K. A. Peterson and J. G. Hill, *Annu. Rep. Comput. Chem.*, 2018, **14**, 47–74.
- 88 R. Gulde, P. Pollak and F. Weigend, *J. Chem. Theory Comput.*, 2012, **8**, 4062–4068.
- 89 F. Weigend, *Computational Methods in Lanthanide and Actinide Chemistry*, Wiley, Chichester, 2015, ch. 7, pp. 181–194.
- 90 D. Rappoport, *J. Chem. Phys.*, 2021, **155**, 124102.
- 91 W. Kutzelnigg and W. Liu, *J. Chem. Phys.*, 2005, **123**, 241102.
- 92 W. Liu and W. Kutzelnigg, *J. Chem. Phys.*, 2007, **126**, 114107.
- 93 D. Peng, N. Middendorf, F. Weigend and M. Reiher, *J. Chem. Phys.*, 2013, **138**, 184105.
- 94 Y. J. Franzke and J. M. Yu, *J. Chem. Theory Comput.*, 2022, **18**, 323–343.
- 95 A. D. Rabuck and G. E. Scuseria, *J. Chem. Phys.*, 1999, **110**, 695–700.
- 96 P. Nava, M. Sierka and R. Ahlrichs, *Phys. Chem. Chem. Phys.*, 2003, **5**, 3372–3381.
- 97 V. R. Saunders and I. H. Hillier, *Int. J. Quantum Chem.*, 1973, **7**, 699–705.
- 98 P. Pulay, *Chem. Phys. Lett.*, 1980, **73**, 393–398.
- 99 M. Fang, D. S. Lee, J. W. Ziller, R. J. Doedens, J. E. Bates, F. Furche and W. J. Evans, *J. Am. Chem. Soc.*, 2011, **133**, 3784–3787.
- 100 M. R. MacDonald, J. W. Ziller and W. J. Evans, *J. Am. Chem. Soc.*, 2011, **133**, 15914–15917.
- 101 F. Weigend and R. Ahlrichs, *Phys. Chem. Chem. Phys.*, 2005, **7**, 3297–3305.
- 102 W. C. Martin, R. Zalubas and L. Hagan, *Atomic energy levels—The rare-earth elements*, National Bureau of Standards, Washington DC, 1978.
- 103 L. Brewer, in *Systematics of the Properties of the Lanthanides*, ed. S. P. Sinha, D. Reidel, Dordrecht, 1983, pp. 17–69.
- 104 A. Klamt and G. Schüürmann, *J. Chem. Soc. Perkin Trans. 2*, 1993, 799–805.
- 105 D. Rappoport and F. Furche, *J. Chem. Phys.*, 2010, **133**, 134105.
- 106 J. D. Rinehart and J. R. Long, *Chem. Sci.*, 2011, **2**, 2078–2085.
- 107 D. N. Woodruff, R. E. Winpenny and R. A. Layfield, *Chem. Rev.*, 2013, **113**, 5110–5148.
- 108 P. C. Stamp and A. Gaita-Ariño, *J. Mater. Chem.*, 2009, **19**, 1718–1730.
- 109 E. Coronado, *Nat. Rev. Mater.*, 2019, **5**, 87–104.
- 110 M. H. Werts, *Sci. Prog.*, 2005, **88**, 101–131.
- 111 J.-C. G. Bünzli and S. V. Eliseeva, *Lanthanide Luminescence: Photophysical, Analytical and Biological Aspects*, Springer, Berlin Heidelberg, 2011, ch. 1, pp. 1–45.
- 112 T. J. Mueller, M. E. Fieser, J. W. Ziller and W. J. Evans, *Chem. Sci.*, 2011, **2**, 1992–1996.
- 113 J. D. Rinehart, M. Fang, W. J. Evans and J. R. Long, *Nat. Chem.*, 2011, **3**, 538–542.

- 114 J. D. Rinehart, M. Fang, W. J. Evans and J. R. Long, *J. Am. Chem. Soc.*, 2011, **133**, 14236–14239.
- 115 M. T. Dumas, G. P. Chen, J. Y. Hu, M. A. Nascimento, J. M. Rawson, J. W. Ziller, F. Furche and W. J. Evans, *J. Organomet. Chem.*, 2017, **849–850**, 38–47.
- 116 M. Fang, J. W. Ziller, J. E. Bates, F. Furche and W. J. Evans, *J. Am. Chem. Soc.*, 2012, **134**, 6064–6067.
- 117 D. H. Woen, G. P. Chen, J. W. Ziller, T. J. Boyle, F. Furche and W. J. Evans, *Angew. Chem. Int. Ed.*, 2017, **56**, 2050–2053.
- 118 A.-M. Ariciu, D. H. Woen, D. N. Huh, L. E. Nodaraki, A. K. Kostopoulos, C. A. Goodwin, N. F. Chilton, E. J. McInnes, R. E. Winpenny, W. J. Evans *et al.*, *Nat. Commun.*, 2019, **10**, 3330.
- 119 Y. J. Franzke and F. Weigend, *J. Chem. Theory Comput.*, 2019, **15**, 1028–1043.
- 120 N. J. Wolford, A. Radovic and M. L. Neidig, *Dalton Trans.*, 2021, **50**, 416–428.
- 121 D. N. Huh, J. P. Bruce, S. G. Balasubramani, S. R. Ciccone, F. Furche, J. C. Hemminger and W. J. Evans, *J. Am. Chem. Soc.*, 2021, **143**, 16610–16620.
- 122 J. M. Kasper, T. F. Stetina, A. J. Jenkins and X. Li, *Chem. Phys. Rev.*, 2020, **1**, 011304.
- 123 B. Samal and V. K. Voora, *J. Chem. Theory Comput.*, 2022, **18**, 7272–7285.